Effects of temperature and oxygen partial pressure on electrical conductivity of Fe-doped β -Ga₂O₃ single crystals

Gyunghyun Ryu; Pramod Reddy; Ramón Collazo; ... et. al



Appl. Phys. Lett. 120, 182101 (2022) https://doi.org/10.1063/5.0093588

A CHORUS





CrossMark

Articles You May Be Interested In

Crystal structure and magnetism of LaCo_{13-x-y}Fe_xSi_y compounds

Journal of Applied Physics (July 1996)

Front Matter for Volume 951

AIP Conference Proceedings (November 2007)

High-resolution dislocation imaging and micro-structural analysis of HVPE- β Ga $_2$ O $_3$ films using monochromatic synchrotron topography

APL Mater (December 2018)





Downloaded from http://pubs.aip.org/aip/apl/article-pdf/doi/10.1063/5.0093588/16447038/182101_1_online.pdf

Effects of temperature and oxygen partial pressure on electrical conductivity of Fe-doped β -Ga₂O₃ single crystals

Cite as: Appl. Phys. Lett. 120, 182101 (2022); doi: 10.1063/5.0093588 Submitted: 29 March 2022 · Accepted: 15 April 2022 · Published Online: 4 May 2022









Gyunghyun Ryu, ¹ 🕞 Pramod Reddy, ² 🅞 Ramón Collazo, ² and Elizabeth C. Dickey^{3, a}l 🕞



AFFILIATIONS

- Department of Materials Science and Engineering, The Pennsylvania State University, University Park, Pennsylvania 16801, USA
- 2 Materials Science and Engineering, North Carolina State University, Raleigh, North Carolina 27607, USA
- ³Department of Materials Science and Engineering, Carnegie Mellon University, Pittsburgh, Pennsylvania 15213, USA

ABSTRACT

In this work, we measure DC and AC conductivity and Hall voltage to determine the origin of electrical insulating properties of Fe-doped β -Ga₂O₃ single crystals, which are measured perpendicular to the $(\overline{2}01)$ crystallographic plane. We find that electrical conduction is predominantly controlled by free electrons in the temperature range 230-800 °C with the mutual compensation of the impurity donor (Si) and acceptor dopant (Fe), explaining the low concentration of free electrons and Fermi level pinning over a wide range of temperatures. Furthermore, the negative temperature-dependence of the carrier mobility indicates that it is limited by optical phonon scattering. Importantly, we find electrical conductivity to be largely independent of oxygen partial pressure (pO_2) from air to 10^{-4} atm at 600 °C, but it becomes slightly dependent on pO₂ at 800 °C, as intrinsic non-stoichiometric point defects begin to influence the charge balance.

Published under an exclusive license by AIP Publishing. https://doi.org/10.1063/5.0093588

Early studies on equilibrium electrical conductivity of undoped polycrystalline β -Ga₂O₃ demonstrated a strong pO₂-dependence as shown in Fig. 1, which is typical for electronically conducting metal oxides. Sasaki and Hijikata¹ and Fleischer et al.² showed that hightemperature electrical conductivity (σ) of unintentionally doped β -Ga₂O₃ ceramics and thin films has pO_2 -dependence of $\sigma \propto pO_2^$ with an activation energy of 1.85-2.1 eV from 800 to 1000 °C. pO2dependent electrical conductivity was attributed to singly charged oxygen vacancies and/or doubly ionized gallium interstitials. Also studying unintentionally doped polycrystalline β-Ga₂O₃, Cojocaru and Prodan³ observed that electrical conductivity was a function of -1/4.55 power of pO₂ at 127 °C and became less pO₂-dependent with increasing temperature. At 727 °C, the $\sigma \propto p O_2^{-1/3.73}$ relation was obtained. The pO2-dependence at various temperatures was attributed to triply charged gallium interstitials. A recent study by Ohya et al. in 2021 showed that unintentionally doped β-Ga₂O₃ ceramics followed the $\sigma \propto p O_2^{-1/4}$ relationship at the high $p O_2$ regime; however, conductivity became less dependent on pO2 in the highly reducing atmosphere. Similar to early studies, formation of doubly ionized gallium interstitials was considered as a possible defect compensation mechanism for $\sigma \propto p O_2^{-1/4}$; however, no other defect models were not proposed for the highly reduced pO2 regime.4

These prior studies on high-temperature equilibrium conductivity argued that n-type conductivity of polycrystalline β -Ga₂O₃ could be explained by simplified defect models with intrinsic point defects. However, the hypotheses were made with no consideration of background impurities and grain boundary effects, where both are important factors determining electrical conductivity vs pO2 in polycrystalline oxides. 5-7 Specifically for β -Ga₂O₃, modern density functional theory (DFT) calculations by Zacherle et al. showed that a small amount of background donors (10 ppm, or $10^{18} \, \mathrm{cm}^{-3}$) can give rise to n-type conductivity, and the relation $\sigma \propto p O_2^{-1/4}$ cannot be driven by a simple defect compensation mechanism. In addition, these DFTbased studies showed that electrical conductivity is pO2-dependent with a 1/6 exponent, i.e., $\sigma \propto pO_2^{-1/6}$ in pure β -Ga₂O₃ due to the doubly ionized oxygen vacancy. Moreover, another DFT calculation by Varley et al. predicted that the origin of n-type conductivity is attributed to the background impurities such as Si or Sn acting as shallow donors, and the oxygen vacancies are deep donors.8 These DFT calculations put into question the inferences made about the dominant defect chemistry from prior experimental literature based on polycrystalline β -Ga₂O₃.

While these aforementioned experimental and theoretical 7,8,12 studies have explored the electrical conduction mechanisms of

a) Author to whom correspondence should be addressed: ecdickey@cmu.edu

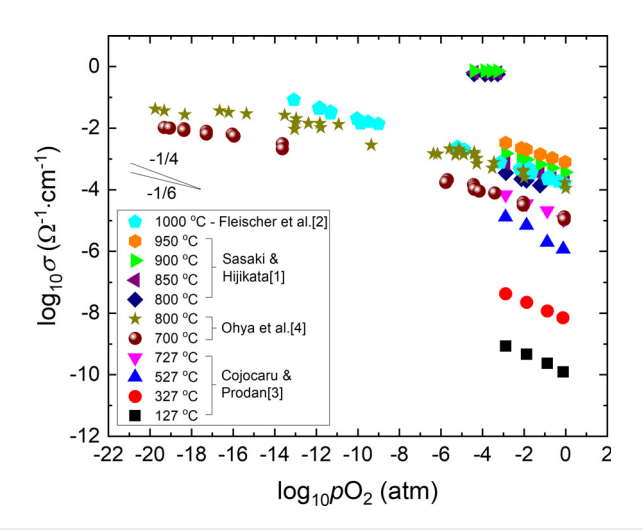


FIG. 1. Electrical conductivity vs oxygen partial pressure in unintentionally doped $\beta\text{-Ga}_2\text{O}_3$ polycrystalline.

unintentionally doped and donor doped n-type β -Ga₂O₃, a clear understanding of the electrical conduction mechanism in semi-insulating β -Ga₂O₃ has not been established. Moreover, many challenges for fabricating p-type β -Ga₂O₃ have been addressed by the community, ^{13,14} motivating a fundamental study of the β -Ga₂O₃ defect chemistry. In addition, the lattice defect chemistry is also

important to understand as it relates to electrical degradation associated with charged ionic defect migration, which may happen under a high electric field during device operation as often observed in perovskite oxide dielectrics. ^{15–18}

In this work, we have investigated the origin of the semi-insulting electrical properties of Fe-doped $\beta\text{-}\mathrm{Ga}_2\mathrm{O}_3$ single crystals. Four-point-probe DC and AC electrical conductivities were measured over a wide range of temperatures in air. Hall characteristics were measured to determine the carrier type, its concentration, and mobility as a function of temperature. In addition, DC electrical conductivity as a function of $p\mathrm{O}_2$ was measured at high-temperatures and discussed in terms of equilibrium defect chemistry.

(010) Fe-doped $\beta\text{-}Ga_2O_3$ single crystals prepared by the edge-defined film-fed growth method (EFG) were purchased from Tamura Corporation (Japan). Prior glow discharge mass spectrometry (GDMS) analysis revealed the unintentional background impurity concentration of Si to be $1\times10^{17}\,\text{cm}^{-3}$ and the intentionally doped Fe concentration to be $8\times10^{17}\,\text{cm}^{-3}$, and thus, the nominal composition in this study is $(Ga_{2\text{-}x\text{-}y}Fe_xSi_y)O_3$ with $x=0.004\,23\,\text{mol}$. % and $y=0.000\,529\,\text{mol}$. %. As shown in Figs. 2(a) and 2(b), four linear platinum (Pt) contacts (500 nm in thickness) spaced by 2–3 mm in length were deposited on the top, bottom, and two sides of a specimen having 20 mm (length) \times 10 mm (width) \times 0.5 mm (thickness) using a DC sputtering system. This configuration was utilized to characterize the AC and DC electrical properties along the in-plane crystallographic direction perpendicular to $(\overline{2}01)$. DC electrical conductivity was measured using a linear two-point-probe and four-point-probe methods

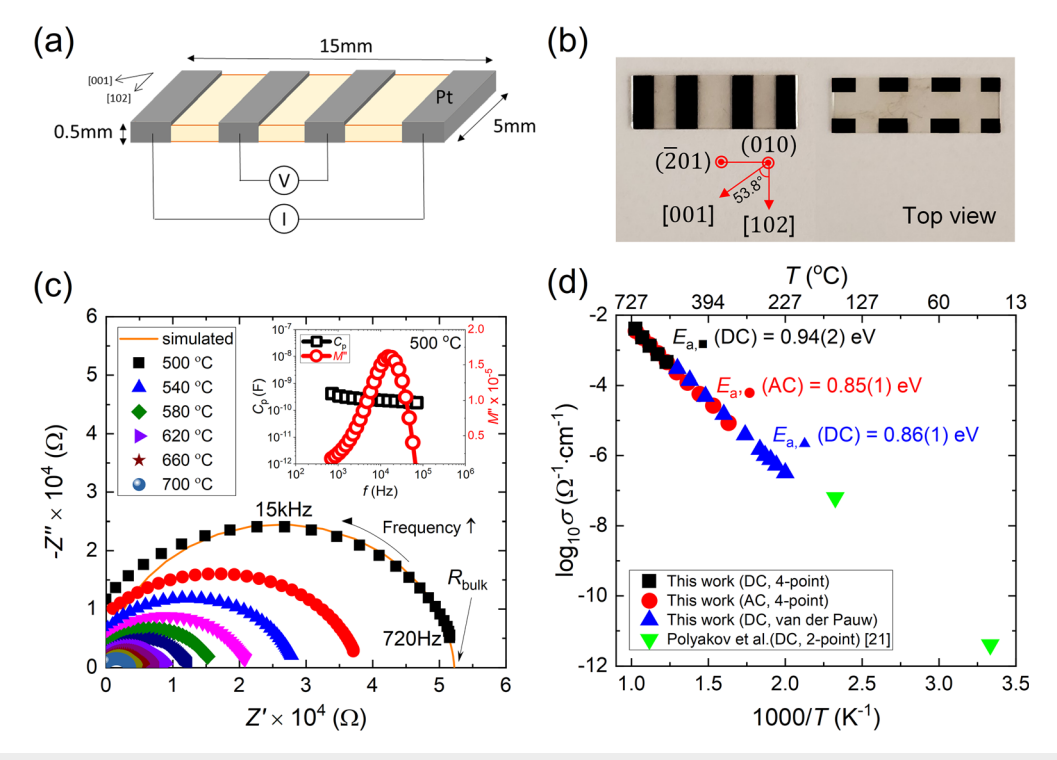


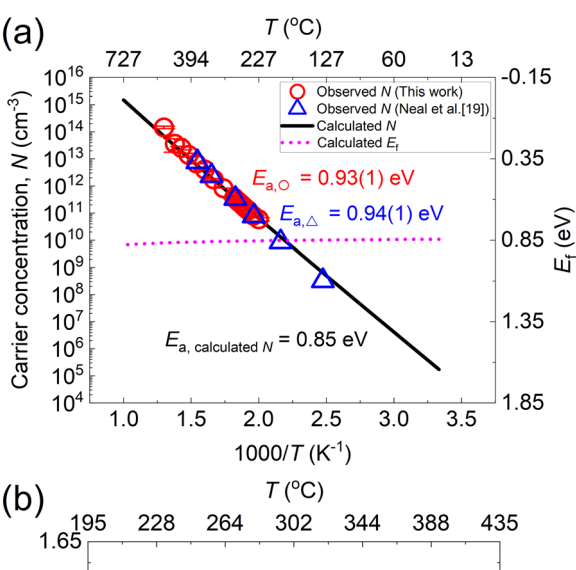
FIG. 2. (a) Schematic of the (010) Fe-doped Ga₂O₃ single crystal with Pt electrodes for four-point-probe DC and AC measurements. (b) Top view of single crystals. Left for DC/AC and right for Hall measurements. (c) Temperature-dependent electrical conductivities. (d) Cole—Cole plots vs temperature in air and capacitance and the imaginary part of modulus as a function of frequency at 500 °C in the inset.

with a Keithley 2000 (Agilent) digital multimeter under a test current between 700 and 10 μ A. The four-terminal AC impedance technique was used to characterize the frequency-dependent electrical properties using a HP4192A (Agilent) impedance analyzer over a frequency range of 5 Hz–5 MHz with a 0.1 V amplitude oscillation. Oxygen partial pressure (pO_2) was controlled from 1 to 10^{-4} atm by changing the gas flow of O_2 and Ar, and the actual pO_2 was monitored by a zirconia oxygen sensor (Ceramic Oxide Fabricators, Australia). Hall measurements were carried out from 225 to 500 °C in a N_2 atmosphere using the van der Pauw method with \sim 200 nm Ti electrodes on top of the sample as shown in Fig. 2(b).

Two-point-probe and four-point-probe DC conductivities were monitored as a function of time at a temperature range of 540–700 °C in air. The conductivities showed less than 1% change in magnitude for several hundred to a few thousand seconds under the bias at a given temperature. As shown in Fig. 2(c), DC conductivity with the two-point-probe geometry exhibited lower magnitude with higher activation energy than the four-point measurements. This difference arose from the fact that in the two-point-probe measurements, the contact resistance was significant compared to the bulk resistance and limits the total electrical conductivity below 650 °C.

Figure 2(d) presents the imaginary (-Z'') vs the real (Z') part of the AC impedance, or Cole-Cole plot, of a Fe-doped β-Ga₂O₃ single crystal as a function of temperature in air measured by the four-wire AC technique. One semi-circle was obtained from 500 to 700 °C, and a partial semi-circle was observed below 500 to 300 °C. At a given temperature, we observed a capacitance plateau with a single response in the imaginary part of the modulus as a function of frequency as shown in the inset in Fig. 2(d). Cole–Cole plots were fitted by a simple equivalent circuit model having a parallel resistance (R) and a constant phase element (CPE) in capacitance. Although the frequency response originates from the homogenous single crystal, a constant phase element (CPE) in capacitance was used rather than a perfect capacitance (C) due to the instrumental artifacts during the four-terminal AC measurement.²⁰ Electrical conductivity obtained from the Cole-Cole plots shows a positive temperature dependence with 0.85(1) eV activation energy in air as shown in Fig. 2(c). The temperature-dependent electrical conductivity from the AC fitting is directly compared to the four-point-probe DC electrical conductivity in Fig. 2(c). The magnitude of electrical conductivity and the activation energies agreed between the different techniques. The activation energies are consistent with the values reported at lower temperatures.²¹ These observations and Ohmic behavior in the current-voltage response indicate that the conductivity of the material is measured by four-terminal AC conductivity with negligible contribution from contact resistances.

Low-temperature electrical characteristics were further analyzed by van der Pauw Hall measurements. As shown in Fig. 3(a), a carrier concentration of $\sim\!\!6\times10^{10}/\mathrm{cm}^3$ at 230 °C following an Arrhenius behavior with an activation energy of 0.93(1) eV with a negative Hall coefficient was observed, agreeing with the prior work. In addition, the Hall mobility shows a negative temperature dependence with a $\sim\!\!1.4(1)$ slope in the $\log_{10}\mu$ vs $\log_{10}T$ plot in Fig. 3(b). The optical phonon scattering may induce a $T^{-1.5}$ power law dependence of mobility, similar to acoustic phonons at higher temperatures where the thermal energy is larger than the optical phonon energy. Since the Hall measurement studies were conducted at temperatures $>\!\!230\,^{\circ}\mathrm{C}$ (500 K),



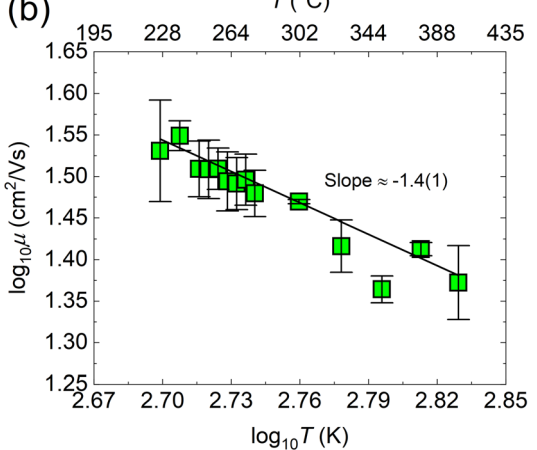


FIG. 3. (a) Carrier concentration and Fermi level referenced to the conduction band and (b) mobility vs temperature.

the power law dependence is due to lattice scattering in general and likely dominated by optical phonons.²²

Low-temperature electrical conductivity obtained by resistivity measurements with van der Pauw geometry is compared to high temperature DC and AC measurements as shown in Fig. 2(c). The electrical conductivities are well matched, and they increase exponentially with increasing temperature from 230 to $700\,^{\circ}$ C, indicating that electrical conductivity Fe-doped β -Ga₂O₃ is governed by one electrical conduction mechanism over this temperature range. In addition, the carrier type was confirmed to be free electrons in the conduction band

To further understand the temperature-dependent carrier concentration, a charge neutrality equation [Eq. (1)] was utilized to predict the concentrations of ionized defects and electronic carriers using the thermodynamic parameters listed in Table I

$$n + N_{\rm A}^- = p + N_{\rm D}^+,$$
 (1)

where $n,p,N_{\rm A}^-$, and $N_{\rm D}^+$ are the concentration of electron, hole, ionized acceptor, and ionized donor, respectively, which can be defined as

TABLE I. Thermodynamic parameters for solving a charge neutrality equation.

Parameter	Symbol	Value	Reference
Density of state in the conduction band	$N_{\rm C}$ (/cm ³)	$7.15 \times 10^{14} \times T^{1.5}$	36
Density of state in the valence band	$N_{\rm V}$ (/cm ³)	$4.15 \times 10^{16} \times T^{1.5}$	
Band gap	$E_{\rm g}$ (eV)	4.85	26
Ionization level of Fe	$E_{\rm g} - E_{\rm acc}$ (eV)	0.78	25
Ionization level of Si	$E_{\rm g} - E_{\rm dn} ({\rm eV})$	0.03	19
Fe concentration	$N_{\rm A}$ (/cm ³)	8×10^{17}	
Si concentration	$N_{\rm D}$ (/cm ³)	1×10^{17}	

$$n = N_{\rm C} \exp\left(-\frac{E_{\rm C} - E_{\rm F}}{kT}\right),\tag{2}$$

$$p = N_{\rm V} \exp\left(-\frac{E_{\rm F} - E_{\rm V}}{kT}\right),\tag{3}$$

$$N_{\rm A}^- = \frac{N_{\rm A}}{1 + 4 \exp\left[(E_{\rm A} - E_{\rm F})/kT\right]},$$
 (4)

$$p = N_{\rm V} \exp\left(-\frac{E_{\rm F} - E_{\rm V}}{kT}\right), \tag{3}$$

$$N_{\rm A}^{-} = \frac{N_{\rm A}}{1 + 4 \exp\left[(E_{\rm A} - E_{\rm F})/kT\right]}, \tag{4}$$

$$N_{\rm D}^{+} = \frac{N_{\rm D}}{1 + 0.5 \exp\left[(E_{\rm F} - E_{\rm D})/kT\right]}, \tag{5}$$

where $N_{\rm C}$ and $N_{\rm V}$ are the effective density of states in the conduction band and valence band, respectively. $E_{\rm C}$ and $E_{\rm V}$ are the bottom of the conduction band and the top of the valence band, respectively. $E_{\rm F}$ is the Fermi level, and k and T are, respectively, the Boltzmann constant and temperature. E_A and E_D are the ionization level for Fe_{Ga}^0 to Fe_{Ga}^{-1} (0/-1) and for Si_{Ga}^0 to Si_{Ga}^{+1} (0/+1), respectively. N_A and N_A^- are the total and ionized concentration of Fe. N_D and N_D^+ are the total and ionized concentration of Si. The degeneracy factors (g) have been chosen to be 1/2 and 4 for Si donors and Fe acceptors, respectively. It is noted that the degeneracy factors are not well established for Ga₂O₃. However, based on the s-orbital nature of the conduction band²³ and Si being singly occupied as an uncharged donor (Si_{Ga}^0/Si_{Ga}^{+1}) (0/+1), the assumption of g = 1/2 may be justified. Fe substitutes Ga in a tetrahedral (albeit distorted) configuration. Although the monoclinic crystal of Ga₂O₃ is different from the diamond crystal structure of Si, Fe is expected to be substitutional in a similar tetrahedral configuration and, hence, symmetry and may be expected to exhibit a similar degeneracy factor as in Si, i.e., 4²⁴ considering the valence band degeneracy in Ga_2O_3 at Γ and M points.²³ Hence for Fe with the acceptor transition (Fe_{Ga}^0/Fe_{Ga}^{-1}) (0/-1), 25 the assumption of a degeneracy factor of 4 may be justified. It has to be further noted that the solution to the charge neutrality expression is insensitive to the magnitude of the degeneracy factors and hence even if the assumed magnitude is off, the conclusions of this work are not affected significantly.

It was assumed in this model that the net positive charge species are the singly ionized Si and holes, and the net negative charge species are the singly ionized Fe and electrons. The compensation mechanism is predominantly due to the charge trapping and de-trapping at the Fe center whose transition level was measured from DLTS measurment to be 0.78 eV from the CBM.²⁵ As shown in Fig. 3(a), this model is in agreement with the observed temperature-dependent carrier concentration Hall measurements. In addition, the Fermi level is pinned to 0.84–0.87 eV over a wide range of temperatures as shown in Fig. 3(a), explaining the observed linear relationship in $\log_{10} \sigma$ vs 1/T. We also calculated the carrier concentration vs temperature using the Fe ionization level of 0.86 eV with $N_{\rm A}/N_{\rm D}$ of 1.65, which were obtained by fitting the observed carrier concentration with a charge neutrality equation in the prior work by Neal et al. 19 The calculated activation energy was 0.93 eV, which is close to the observed activation energy; however, there was a slight discrepancy in magnitude between the observed and calculated carrier concentration; the calculated value is two times higher than the observed carrier concentration.

Although the prediction indicates that the charge compensation mechanism can be explained by only considering the donor (Si) and acceptor (Fe) mutual compensation, we further examined electrical conductivity as a function of pO2 to study a possibility of contribution of intrinsic point defects to the overall charge balance. Considering the phase stability of β -Ga₂O₃,²⁷ four-point-probe DC conductivity was measured from 600 to 820 °C in a pO2 range of 0.21 atm (air) to 10⁻⁴ atm. As soon as pO₂ was changed at a given temperature, fourpoint-probe DC conductivity was monitored as a function of time. Once time-independent conductivity was achieved, the sample was assumed to be chemically equilibrated with respect to pO₂. The sample reached equilibrium in approximately 1-2 h at 600 °C and in less than 1 h at higher temperature (800 °C) after a decrease in pO2 of one decade. The measurements were performed in a O2 and Ar mixture. Thus, it was assumed that hydrogen incorporation with Ga₂O₃ is negligible, and protons do not significantly contribute to the electrical conductivity. As shown in Fig. 4(a), the electrical conductivity shows pO₂-independent behavior at 600 °C over the measurement range. With increasing temperature, conductivity increases modestly with decreasing pO_2 ; however, the dependence is weak in comparison to other multivalent acceptor doped oxide dielectrics at this pO₂ range.²⁸ As shown in Fig. 4(b), an Arrhenius behavior of electrical conductivity is observed at each pO2 condition, and the activation energy changes gradually from 0.92 to $1.04 \,\mathrm{eV}$ with decreasing $p\mathrm{O}_2$.

pO2-independent electrical conductivity can be explained by several defect compensating mechanisms. One mechanism is attributed to the generation of intrinsic point defects such as oxygen vacancies for ionically compensating dopants. This mechanism is generally observed in acceptor-doped oxides, and their defect chemistry has been well established.^{29–31} When ionic compensation dominates such that conductivity is dominated by the ionic species, broad pO₂independent electrical conductivity can be observed. In some cases, judicious choices of multivalent acceptors and donors can override the ionic compensation and pin the Fermi level over broad pO2 ranges as shown for BaTiO₃ in the early studies. ^{32–35} In Fe-doped β -Ga₂O₃ studied here, pO2-independent electrical conductivity is attributed to the pinned Fermi level due to the dominating impurity donor (Si) compensating the acceptor (Fe), and a total electrical conductivity is predominantly governed by the electron conductivity over a broad range of pO_2 . According to DFT calculations, ^{7,8} in reducing conditions, the oxygen vacancy formation energy is the lowest among the native point defects, except for triply ionized gallium interstitials at very low Fermi energies, which are believed to act as deep donors. These DFT calculations suggest a low concentration of intrinsic point defects in β -Ga₂O₃ single crystals. Moreover, Hall measurements and the charge neutrality equation reveal that the Si donor and the Fe acceptor mutual compensation can explain electronic conductivity over a wide range of

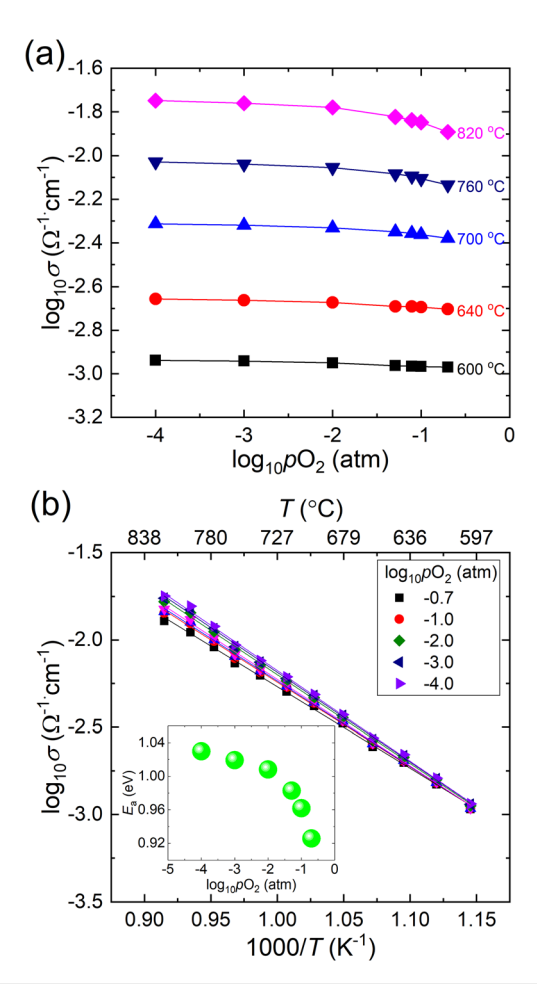


FIG. 4. (a) Oxygen partial pressure dependent DC electrical conductivity at various temperatures. (b) DC electrical conductivity vs temperature with a change in activation energy (inset) at each pO_2 condition.

temperatures. Therefore, semi-insulting pO_2 -independent electrical conductivity of Fe-doped β -Ga₂O₃ is attributed to the donor and multivalent acceptor co-doping mechanism with the low concentration of intrinsic point defects.

It is important to note that with increasing temperature, we observed a slight increase in electrical conductivity along with a transition to a slightly higher activation energy as the sample equilibrates with a reduced pO_2 . This is probably due to a minor additional contribution of electrons generated by intrinsic deeper donors such as oxygen vacancies. The influence of non-stoichiometric lattice defects is not very significant at these measurement conditions since the Fermi level is pinned by Si and Fe; however, the results suggest that there is a possibility of generating nonstoichiometric point defects with further increasing temperature or reducing pO_2 .

In conclusion, the semi-insulating properties of Fe-doped β -Ga₂O₃ single crystals grown via the edge-defined film-fed method were investigated as a function of the temperature and oxygen partial pressure. It was revealed from DC and AC conductivities and Hall measurements that in-plane electrical conductivity perpendicular to

the $(\overline{2}01)$ crystallographic planes follows an Arrhenius behavior from 230 to 800 °C with an activation energy of 0.84–0.94 eV. The Hall measurements showed that the crystal is n-type. While the carrier concentration showed a positive temperature dependence, the mobility exhibited a negative temperature dependence, characteristic of optical phonon scattering. Semi-insulting electrical conductivity was explained by a low electron concentration, which is achieved by donor (Si) and acceptor (Fe) mutual compensation, leading to Fermi level pinning over a wide range of temperatures. DC electrical conductivity vs pO_2 was examined from 600 to 800 °C from air to 10^{-4} atm and showed that conductivity is pO_2 -independent at 600 °C, suggesting a low intrinsic point defect concentration. At higher temperatures, electrical conductivity increased moderately with reducing pO_2 , which is probably due to the generation of electron compensating intrinsic point defects such as oxygen vacancies.

G. H. Ryu and E. C. Dickey gratefully acknowledge partial support from the Air Force Office of Scientific Research under Grant No. FA9550-19-1-0222. P. Reddy and R. Collazo gratefully acknowledge partial support from NSF (No. ECCS-1653383).

AUTHOR DECLARATIONS Conflict of Interest

The authors have no conflicts to disclose.

DATA AVAILABILITY

The data that support the findings of this study are available from the corresponding author upon reasonable request.

REFERENCES

- ¹T. Sasaki and K. Hijikata, Proc. Inst. Nat. Sci., Nihon. Univ. 9, 29 (1974).
- ²M. Fleischer, L. Hollbauer, E. Born, and H. Meixner, J. Am. Ceram. Soc. 80, 2121 (2005).
- ³L. N. Cojocaru and A. Prodan, Rev. Roum. Phys. **19**, 209 (1974).
- ⁴Y. Ohya, H. Kanaoka, S. Iwata, C. Takai-Yamashita, and T. Ban, J. Ceram. Soc. Jpn. **129**, 254 (2021).
- ⁵½. Wu, P. C. Bowes, J. N. Baker, and D. L. Irving, J. Appl. Phys. **128**, 014101 (2020).
- ⁶P. C. Bowes, J. N. Baker, J. S. Harris, B. D. Behrhorst, and D. L. Irving, Appl. Phys. Lett. 112, 022902 (2018).
- ⁷T. Zacherle, P. C. Schmidt, and M. Martin, Phys. Rev. B 87, 235206 (2013).
- ⁸J. B. Varley, J. R. Weber, A. Janotti, and C. G. Van de Walle, Appl. Phys. Lett. 97, 142106 (2010).
- ⁹N. Suzuki, S. Ohira, M. Tanaka, T. Sugawara, K. Nakajima, and T. Shishido, Phys. Status Solidi C 4, 2310 (2007).
- ¹⁰E. G. Villora, K. Shimamura, Y. Yoshikawa, T. Ujiie, and K. Aoki, Appl. Phys. Lett. 92, 202120 (2008).
- ¹¹D. Gogova, G. Wagner, M. Baldini, M. Schmidbauer, K. Irmscher, R. Schewski, Z. Galazka, M. Albrecht, and R. Fornari, J. Cryst. Growth 401, 665 (2014).
- ¹²S. Lany, APL Mater. **6**, 046103 (2018).
- A. Kyrtsos, M. Matsubara, and E. Bellotti, Appl. Phys. Lett. 112, 032108 (2018).
 I. Stepanov, V. I. Nikolasy, V. E. Bougray, and A. E. Pomanov, Pey. Adv.
- ¹⁴S. I. Stepanov, V. I. Nikolaev, V. E. Bougrov, and A. E. Romanov, Rev. Adv Mater. Sci. 44, 63 (2016).
- ¹⁵T. Bayer, J. J. Wang, J. J. Carter, A. Moballegh, J. Baker, D. L. Irving, E. C. Dickey, L. Q. Chen, and C. A. Randall, Acta Mater. 117, 252 (2016).
- ¹⁶J. J. Wang, H. B. Huang, T. J. M. Bayer, A. Moballegh, Y. Cao, A. Klein, E. C. Dickey, D. L. Irving, C. A. Randall, and L. Q. Chen, Acta Mater. 108, 229 (2016).
- ¹⁷D. M. Long, B. Cai, J. N. Baker, P. C. Bowes, T. J. M. Bayer, J. J. Wang, R. Wang, L. Q. Chen, C. A. Randall, D. L. Irving, and E. C. Dickey, J. Am. Ceram. Soc. 102, 3567 (2019).

- ¹⁸R. Waser, T. Baiatu, and K.-H. Härdtl, J. Am. Ceram. Soc. 73, 1654 (1990).
- ¹⁹ A. T. Neal, S. Mou, S. Rafique, H. Zhao, E. Ahmadi, J. S. Speck, K. T. Stevens, J. D. Blevins, D. B. Thomson, N. Moser, K. D. Chabak, and G. H. Jessen, Appl. Phys. Lett. 113, 062101 (2018).
- ²⁰B. W. Veal, P. M. Baldo, A. P. Paulikas, and J. A. Eastman, J. Electrochem. Soc. 162, H47 (2015).
- ²¹ A. Y. Polyakov, N. B. Smirnov, I. V. Shchemerov, S. J. Pearton, F. Ren, A. V. Chernykh, and A. I. Kochkova, Appl. Phys. Lett. 113, 142102 (2018).
- ²²N. Ma, N. Tanen, A. Verma, Z. Guo, T. Luo, H. (Grace) Xing, and D. Jena, Appl. Phys. Lett. **109**, 212101 (2016).
- ²³ M. A. Blanco, M. B. Sahariah, H. Jiang, A. Costales, and R. Pandey, Phys. Rev. B 72, 184103 (2005).
- ²⁴H. I. Ralph, J. Appl. Phys. **49**, 672 (1978).
- ²⁵M. E. Ingebrigtsen, J. B. Varley, A. Yu. Kuznetsov, B. G. Svensson, G. Alfieri, A. Mihaila, U. Badstübner, and L. Vines, Appl. Phys. Lett. 112, 042104 (2018).
- ²⁶C. Janowitz, V. Scherer, M. Mohamed, A. Krapf, H. Dwelk, R. Manzke, Z. Galazka, R. Uecker, K. Irmscher, R. Fornari, M. Michling, D. Schmeißer, J. R. Weber, J. B. Varley, and C. G. Van De Walle, New J. Phys. 13, 085014 (2011).

- ²⁷R. Togashi, K. Nomura, C. Eguchi, T. Fukizawa, K. Goto, Q. T. Thieu, H. Murakami, Y. Kumagai, A. Kuramata, S. Yamakoshi, B. Monemar, and A. Koukitu, Jpn. J. Appl. Phys., Part 1 54, 041102 (2015).
- 28 C. R. Song, H. I. Yoo, and J. Y. Kim, J. Electroceram. 1, 27 (1997).
- ²⁹C. B. Gopal and S. M. Haile, J. Mater. Chem. A **2**, 2405 (2014).
- 30 Y. H. Han, J. B. Appleby, and D. M. Smyth, J. Am. Ceram. Soc. 70, 96 (1987).
- 31 R. Waser, J. Am. Ceram. Soc. 74, 1934 (1991).
- ³²Y. Y. Yeoh, H. Jang, and H. I. Yoo, Phys. Chem. Chem. Phys. **14**, 1642 (2012).
- ³³C. E. Lee, S. H. Kang, D. S. Sinn, and H. I. Yoo, J. Electroceram. 13, 785 (2004).
- 34G. H. Ryu, P. C. Bowes, J. R. McGarrahan, D. L. Irving, and E. C. Dickey, J. Am. Ceram. Soc. 105, 292 (2022).
- 35P. C. Bowes, G. H. Ryu, J. N. Baker, E. C. Dickey, and D. L. Irving, J. Am. Ceram. Soc. 104, 5859 (2021).
- 36The effective density of state in conduction and valence bands was calculated using the effective mass of the electron.